The influence of platinum(IV) ions on the formation of iron oxides in a highly alkaline medium

Stjepko Krehula *, Svetozar Musić

Division of Materials Chemistry, Ruđer Bošković Institute, P.O. Box 180, HR-10002 Zagreb, Croatia

ARTICLE INFO

ABSTRACT

The effect of the presence of platinum(IV) ions, in the form of $Pt(OH)_6^{2-}$ at a high pH, on the formation of iron oxides in a highly alkaline precipitation system was investigated using X-ray powder diffraction (XRD), ^{57}Fe Mössbauer and FT-IR spectroscopies, field emission scanning electron microscopy (FE-SEM) and energy dispersive X-ray spectroscopy (EDS). Monodispersed lath-like α-FeOOH (goethite) particles precipitated by hydrothermal treatment in a highly alkaline medium with the addition of tetramethylammonium hydroxide (TMAH) were used as reference material. In the presence of 1 or 5 mol% of platinum ions in the precipitation system the lath-like α-FeOOH particles were formed as a single phase after a short hydrothermal treatment (2 h). No significant change in the size and shape of these particles in comparison to the reference sample was observed. After 6 h of autoclaving the formation of platinum nanoparticles at the surface of α-FeOOH particles via reduction by TMAH and/or its decomposition products became visible. These nanoparticles acted as a catalyst for the reduction of Fe(III) ions into Fe(II) and gradual transformation of α-FeOOH into a mixed Fe(II)–Fe(III) oxide (Fe_3O_4, magnetite) by the dissolution–recrystallization mechanism. The presence of a higher concentration of platinum ions accelerates the process of α-FeOOH $\rightarrow$ Fe_3O_4 transformation with the appearance of α-Fe$_2O_3$ (hematite) particles as an intermediate product.

© 2010 Elsevier B.V. All rights reserved.

1. Introduction

Natural iron oxides are formed by weathering of iron-rich primary minerals (silicates, spinels), commonly in the presence of cations of other metals besides iron. These foreign cations have a significant influence on the process of iron oxides formation. Thus formed iron oxides usually contain various metal cations incorporated into their structure and in this way play an important role in the availability of these cations in soils [1–6]. Similar to natural iron oxides, the formation of synthetic ones is also strongly impacted by the presence of various metal cations. The addition of varying amounts of these cations may have a drastic impact on the phase composition of formed iron oxides, as well as on the particle size and shape [7–13]. Metal-for-Fe substitution in the structure of synthetic iron oxides, prepared in the presence of corresponding foreign metal cations, has been widely reported, especially in the case of goethite, α-FeOOH [14–18]. Incorporation of various metal cations into the structure of iron oxides can affect their electric [19,20], magnetic [21–24], thermal [23,24], solubility [25], catalytic [26–28], adsorption [29,30], gas sensing [31–33] and other properties.

The formation of synthetic iron oxides in the presence of platinum ions and the possibility of Pt-for-Fe substitution in the iron oxide structure have been poorly investigated. Sudakar et al. [34] used low concentrations of Pt^{4+}, Pd^{2+} or Rh^{3+} as morphology controlling cationic additives for the synthesis of acicular hydrogoethite particles. A thin film of nanocrystalline Pt-doped hematite was prepared by electrodeposition method as a possible active material for photoelectrochemical water splitting [35]. A Pt-doped γ-Fe$_2O_3$ thin film was prepared in order to test gas sensing properties [36]. Pt–Fe$_3O_4$ core–shell nanoparticles were prepared as a precursor for the synthesis of Fe–Pt nanoparticles with remarkable magnetic properties [37].

However, to the best of our knowledge, no systematic investigation of the influence of platinum ions on the formation of α-FeOOH has been published yet. The aim of the present work was to investigate the impact of platinum ions on the formation of α-FeOOH in a highly alkaline medium, with focus on the phase and microstructural properties of precipitation products. Uniform lath-like α-FeOOH particles prepared in our earlier work [38,39] were used as reference material. Low polydispersity of these particles makes them suitable as a model colloid for various applications [40,41], as a component of nanocomposites with improved properties [42], as well as reference material for studies on the influence of cationic additives on the synthesis and properties of α-FeOOH [43–45].

* Corresponding author. Tel.: +385 1 4561 094; fax: +385 1 4680 098.
E-mail address: krehul@irb.hr (S. Krehula).

Table 1

Concentration conditions for the preparation of samples by autoclaving at 160 °C and phase composition of solid samples determined by X-ray powder diffraction.

Sample	[FeCl$_3$] (mol dm^{-3})	[PtCl$_4$] (mol dm^{-3})	$100 \cdot$[Pt]/([Pt] + [Fe])	TMAH[a] (mol dm^{-3})	Aging time (h)	Phase composition[b]
G	0.1	0	0	0.7	2	G
PtG1-2h	0.1	1.01×10^{-3}	1	0.7	2	G
PtG1-6h	0.1	1.01×10^{-3}	1	0.7	6	G
PtG1-16h	0.1	1.01×10^{-3}	1	0.7	16	G + M
PtG1-24h	0.1	1.01×10^{-3}	1	0.7	24	M + G + Pt
PtG1-72h	0.1	1.01×10^{-3}	1	0.7	72	M + Pt
PtG2-2h	0.1	5.27×10^{-3}	5	0.7	2	G
PtG2-6h	0.1	5.27×10^{-3}	5	0.7	6	G + Pt
PtG2-16h	0.1	5.27×10^{-3}	5	0.7	16	M + Pt + G + H
PtG2-24h	0.1	5.27×10^{-3}	5	0.7	24	M + Pt

[a] TMAH = tetramethylammonium hydroxide (25% w/w).
[b] G = goethite (α-FeOOH), H = hematite (α-Fe$_2$O$_3$), M = magnetite (Fe$_3$O$_4$).

2. Experimental

2.1. Preparation of samples

Iron(III) chloride hexahydrate (FeCl$_3$·6H$_2$O) of analytical purity, supplied by *Kemika*, platinum(IV) chloride (PtCl$_4$), supplied by *Merck,* and a tetramethylammonium hydroxide (TMAH) solution (25% w/w, electronic grade 99.9999%) supplied by *Alfa Aesar®*, were used. Twice-distilled water prepared in our own laboratory was used in all experiments. Predetermined volumes of FeCl$_3$ and PtCl$_4$ solutions and twice-distilled water were mixed, then TMAH was added as a precipitating agent. The exact experimental conditions
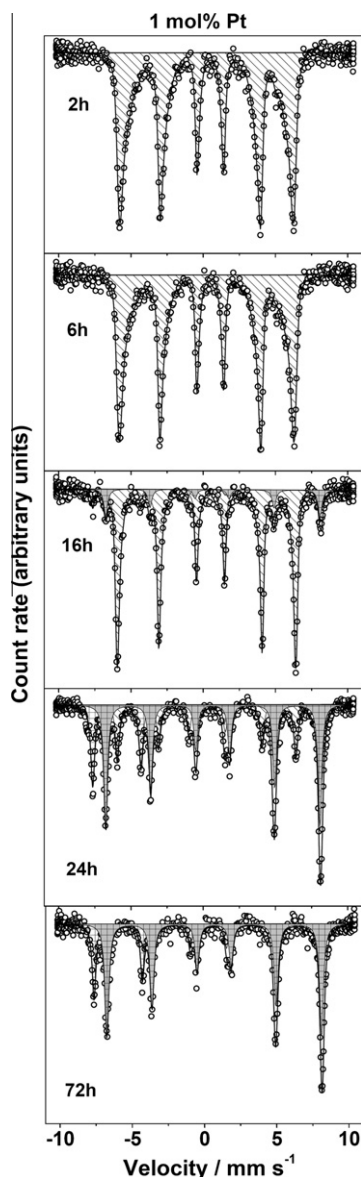
Fig. 1. ^{57}Fe Mössbauer spectra (recorded at 20 °C) of samples obtained after various heating periods in the presence of 1 mol% Pt.
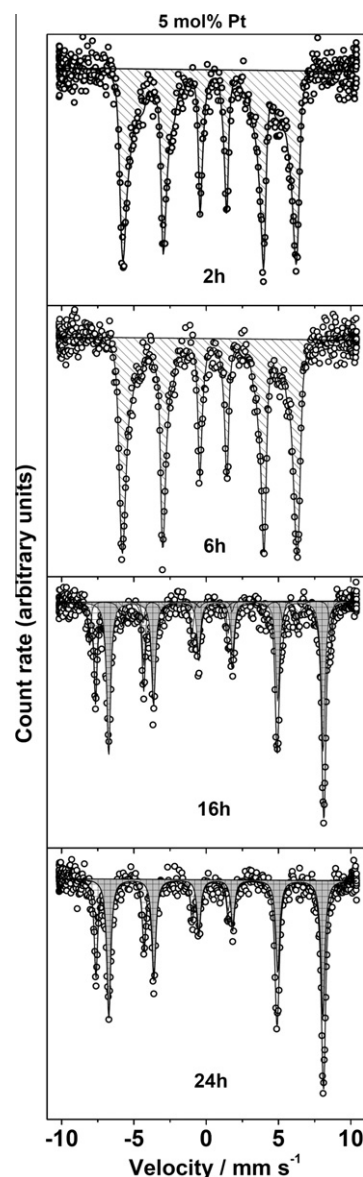
Fig. 2. ^{57}Fe Mössbauer spectra (recorded at 20 °C) of samples obtained after various heating periods in the presence of 5 mol% Pt.

Table 2
^{57}Fe Mössbauer parameters calculated for iron oxide samples formed in the presence of various amounts of Pt(IV) ions.

Sample	Spectral line	δ (mm s^{-1})	2ε (mm s^{-1})	$\langle B_{hf} \rangle^*$ or B_{hf} (T)	Γ (mm s^{-1})	Area (%)	Identification
G	M	0.37	−0.26	34.5*	0.24	100	α-FeOOH
PtG1-2h	M	0.37	−0.26	34.5*	0.25	100	α-FeOOH
PtG1-6h	M	0.37	−0.26	35.1*	0.23	100	α-FeOOH
PtG1-16h	M$_1$	0.37	−0.27	36.5*	0.21	83.8	α-FeOOH
	M$_2$	0.66	0.01	46.0	0.31	10.6	Fe$_3$O$_4$–Fe(II)/Fe(III) octahedral sites
	M$_3$	0.28	0.02	49.2	0.27	5.6	Fe$_3$O$_4$–Fe(III) tetrahedral sites
PtG1-24h	M$_1$	0.37	−0.26	38.3	0.27	18.1	α-FeOOH
	M$_2$	0.66	0.01	46.0	0.34	52.2	Fe$_3$O$_4$–Fe(II)/Fe(III) octahedral sites
	M$_3$	0.27	−0.01	49.0	0.30	29.7	Fe$_3$O$_4$–Fe(III) tetrahedral sites
PtG1-72h	M$_1$	0.66	0.01	46.1	0.33	64.1	Fe$_3$O$_4$–Fe(II)/Fe(III) octahedral sites
	M$_2$	0.28	−0.01	49.1	0.30	35.9	Fe$_3$O$_4$–Fe(III) tetrahedral sites
PtG2-2h	M	0.37	−0.27	34.1*	0.24	100	α-FeOOH
PtG2-6h	M	0.37	−0.25	35.2*	0.27	100	α-FeOOH
PtG2-16h	M$_1$	0.37	−0.26	37.7	0.40	8.5	α-FeOOH
	M$_2$	0.37	−0.20	51.7	0.23	8.7	α-Fe$_2$O$_3$
	M$_3$	0.66	0.02	46.0	0.31	54.9	Fe$_3$O$_4$–Fe(II)/Fe(III) octahedral sites
	M$_4$	0.27	0.00	49.1	0.25	27.8	Fe$_3$O$_4$–Fe(III) tetrahedral sites
PtG2-24h	M$_1$	0.67	0.00	45.9	0.32	62.3	Fe$_3$O$_4$–Fe(II)/Fe(III) octahedral sites
	M$_2$	0.28	−0.01	49.0	0.28	37.7	Fe$_3$O$_4$–Fe(III) tetrahedral sites

Errors: δ = ±0.01 mm s^{-1}, 2ε = ±0.01 mm s^{-1}, B_{hf} = ±0.2 T.
Isomer shift is given relative to α-Fe.
* Hyperfine magnetic field distribution.
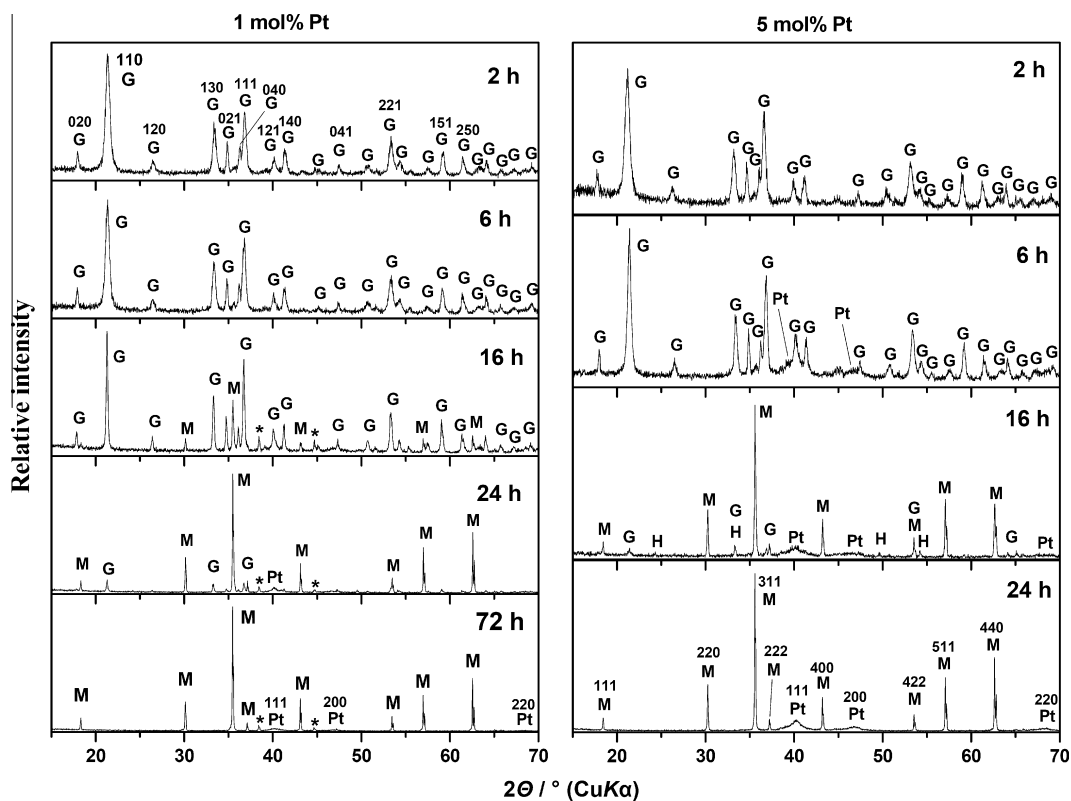
Fig. 3. XRD patterns of obtained powder samples, recorded at 20 °C (G = α-FeOOH, M = Fe$_3$O$_4$, H = α-Fe$_2$O$_3$, Pt = Platinum, ∗ = Al-holder).

Table 3
Unit cell parameters and the mean crystallite size for pure and Pt-substituted α-FeOOH phase in the selected samples.

Sample	100·[Pt]/([Pt] + [Fe])	Unit cell parameter (Å)			V (Å^3)	Mean crystallite size (nm)		
		a	b	c		a-Axis	b-Axis	c-Axis
G	0	4.614(1)	9.954(7)	3.022(0)	138.8(1)	18(1)	43(1)	>71
PtG1-2h	1	4.615(1)	9.953(6)	3.022(0)	138.8(1)	14(1)	26(1)	>42
PtG2-2h	5	4.617(1)	9.950(6)	3.024(0)	138.9(1)	13(1)	22(1)	>35

for sample preparation are given in Table 1. Thus formed aqueous suspensions were vigorously shaken for ~10 min, then heated at 160 °C, using the Parr general-purpose bomb (model 4744) com-

prising a Teflon vessel and a cup. After the proper heating time the precipitates were cooled to room temperature (the mother liquor pH ≈ 13.5) and subsequently washed with twice-distilled

water to remove "neutral electrolyte". The ultraspeed *Sorvall* RC2-B centrifuge was used. After drying all precipitates were characterized by X-ray powder diffraction, Mössbauer and FT-IR spectroscopies, as well as high-resolution scanning electron microscopy. The molar percentages of iron and platinum in the particles were determined by EDS analysis.

2.2. Instrumentation

[57]Fe Mössbauer spectra were recorded in the transmission mode using a standard *WissEl* (Starnberg, Germany) instrumental configuration. A [57]Co/Rh Mössbauer source was used. The velocity scale and all data refer to the metallic α-Fe absorber at 20 °C. A quantitative analysis of the recorded spectra was made using the *MossWinn* program.

X-ray powder diffractometer APD 2000 (Cu Kα radiation, graphite monochromator, NaI-Tl detector) manufactured by *Ital-Structures* (Riva Del Garda, Italy) was used. The selected samples were mixed with about 10% KBr (for IR-spectroscopy, supplied by *Fluka*) as an internal standard. The exact positions and full width at half maximum (FWHM) values of the diffraction lines were obtained by fitting a pseudo-Voigt function to experimental data using the *WinDust32* program (*ItalStructures*). The unit cell dimensions were calculated from the positions of lines 020, 110, 130, 021, 111, 121, and 140 using the XLAT least squares program [46]. The mean crystallite sizes along the crystallographic axes were estimated from the line broadening of the X-ray diffraction lines, after correcting the measured full width at half maximum (FWHM) for instrumental broadening, using the Scherrer equation and procedure described by Schulze and Schwertmann [47]. The Scherrer equation assigns all line broadening to crystallite size and does not take into account line broadening caused by lattice strains or other imperfections [48].

Fourier transform infrared (FT-IR) spectra were recorded at RT using a *Perkin–Elmer* spectrometer (model 2000). The FT-IR spectrometer was connected to a PC with the installed IRDM (IR data manager) program to process the recorded spectra. The specimens were pressed into small discs using a spectroscopically pure KBr matrix.
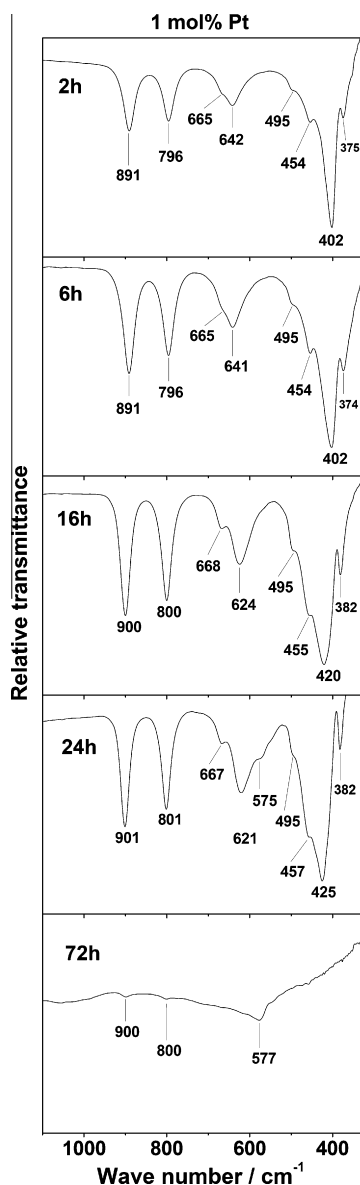
Fig. 4. FT-IR spectra (recorded at RT) of samples obtained after various heating periods in the presence of 1 mol% Pt.
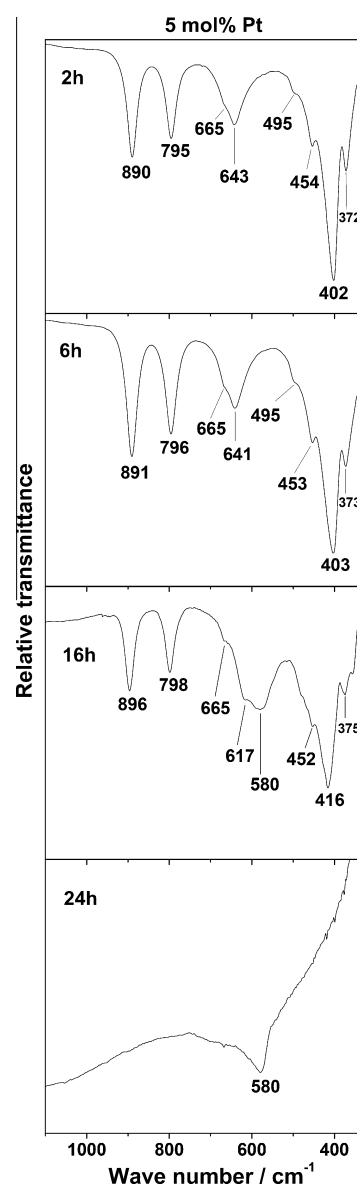
Fig. 5. FT-IR spectra (recorded at RT) of samples obtained after various heating periods in the presence of 5 mol% Pt.

A thermal field emission scanning electron microscope (FE-SEM, model JSM-7000F, manufactured by *JEOL Ltd.*) was used. FE-SEM was linked to the EDS/INCA 350 (energy dispersive X-ray analyser) manufactured by *Oxford Instruments Ltd.* The specimens were not coated with an electrically conductive surface layer.

3. Results and discussion

3.1. ^{57}Fe Mössbauer spectroscopy

The Mössbauer spectra of synthesized samples are shown in Figs. 1 and 2, while the calculated Mössbauer parameters and phase identification are given in Table 2.

The spectrum of the sample obtained after 2 h of hydrothermal treatment in the presence of 1 mol% of Pt ions (sample PtG1-2h, Fig. 1) is a typical asymmetrical sextet corresponding to α-FeOOH of medium crystallinity, almost identical to the spectrum of the reference sample G [49]. The Mössbauer spectrum of goethite recorded at room temperature may vary from a well-shaped sextet to a paramagnetic doublet in dependence on the particle size and crystallinity [50]. The Mössbauer spectrum of goethite is also very sensitive to the incorporation of metal cations into the crystal structure. The main feature of this effect in the corresponding Mössbauer spectra is a decrease in hyperfine magnetic field (HMF) [16,51,52]. The sextet corresponding to α-FeOOH in the Mössbauer spectra of obtained samples was fitted taking into account the HMF distribution. The average HMF in the sample PtG1-2h was not reduced in comparison with the reference sample (Table 2), which indicates no significant incorporation of Pt ions into the structure of α-FeOOH.

Further hydrothermal treatment of the precipitation system (for 6, 16 and 24 h) caused the narrowing of the lines in α-FeOOH sextets in the Mössbauer spectra of obtained samples (Fig. 1). Average HMF was increased (Table 2) due to an improvement in crystallinity by dissolution or aggregation of smaller α-FeOOH particles with simultaneous growth of larger ones having fewer imperfections [39]. Besides, the sextet corresponds to α-FeOOH, two characteristic Fe_3O_4 sextets are visible in the spectra of samples PtG1-16h and PtG1-24h. The outer sextet of the smaller area corresponds to Fe(III) in tetrahedral sites and the inner sextet of the larger area corresponds to Fe(III) and Fe(II) in octahedral sites [50,53]. The area of these sextets increases with the prolongation of the hydrothermal treatment, which indicates a gradual transformation of α-FeOOH to Fe_3O_4. This transformation is completed in the sample obtained after 72 h – only Fe_3O_4 sextets are present in the corresponding Mössbauer spectrum.

The presence of 5 mol% of Pt ions during the hydrothermal treatment brought about a slight reduction of the average HMF in α-FeOOH (Table 2, sample PtG2-2h), which indicates the possibility of Pt ions being incorporated into the α-FeOOH structure. A higher concentration of Pt ions accelerated the α-FeOOH to Fe_3O_4 transformation. The Mössbauer spectrum of the sample obtained after 24 h of hydrothermal treatment shows only the presence of characteristic Fe_3O_4 sextets (Fig. 2). A small amount of hematite was detected in sample PtG2-16h, based on the presence of a characteristic hematite sextet of low intensity in the corresponding Mössbauer spectrum (Fig. 2).

3.2. X-ray powder diffraction

Crystalline phases were determined (Table 1) from the recorded XRD patterns (Fig. 3) using JCPDS PDF cards No. 29-713 for α-FeOOH, No. 33-664 for α-Fe_2O_3, No. 19-629 for Fe_3O_4 and No. 4-0802 for platinum. Unit cell parameters, calculated from the positions of the corresponding diffraction lines, and the mean crystallite size

of α-FeOOH for samples G, PtG1-2h and PtG2-2h are given in Table 3.

XRD patterns of the samples obtained after 2 h of hydrothermal treatment (Fig. 3) confirmed the result obtained by Mössbauer spectroscopy that α-FeOOH as a single phase was formed in the presence of 1 or 5 mol% of Pt ions. However, the presence of Pt ions in the precipitation system led to the broadening of diffraction lines (Fig. 3) due to the formation of α-FeOOH crystallites of lower
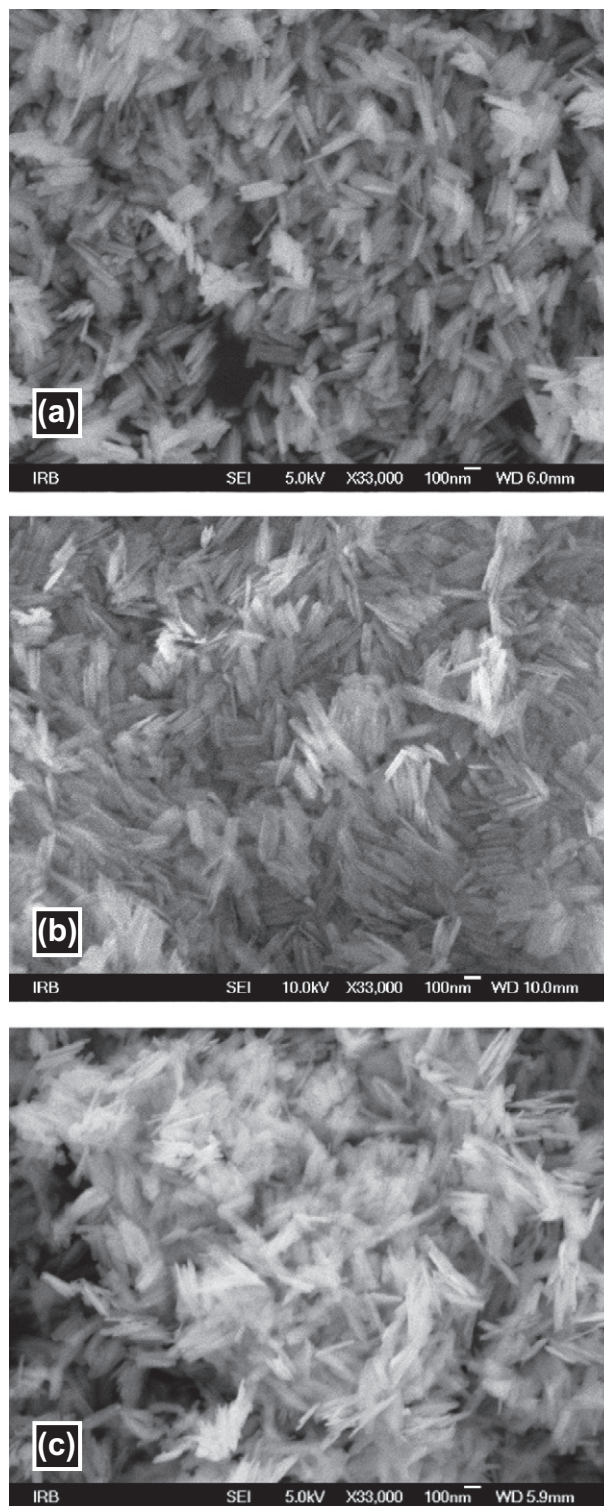
Fig. 6. FE-SEM images of samples: (a) reference sample G, (b) PtG1-2h and (c) PtG2-2h.

mean crystallite size (Table 3). This decrease of crystallite size is responsible for the reduction of HMF (Table 2, sample PtG2-2h). Unit cell dimensions were only slightly changed (Table 3) due to similar ionic radii of iron(+3) and platinum(+4) ions (0.645 and 0.625 Å, respectively [54]) and a minor Pt-for-Fe substitution into the α-FeOOH structure.

Continued hydrothermal treatment of the precipitation system (for 6 and 16 h) led to the narrowing of the α-FeOOH diffraction lines due to improved crystallinity. The diffraction lines of Fe_3O_4 appeared in the samples obtained after 16 h of treatment; intensity of these lines was stronger for the sample formed in the presence of a higher concentration of Pt ions, which indicates a faster α-FeO-OH to Fe_3O_4 transformation. XRD results confirmed the results obtained by Mössbauer spectroscopy, i.e., that the α-FeOOH to Fe_3O_4 transformation was completed in the sample obtained after 72 h in the presence of 1 mol% of Pt ions and in the sample obtained after 24 h in the presence of 5 mol% of Pt ions.

The presence of very broad diffraction lines corresponding to metallic platinum (Pt^0, cubic crystal system, space group $Fm\bar{3}m$) indicates the formation of nanosize crystallites of that metal during the hydrothermal treatment. XRD lines characteristic of α-Fe_2O_3 in the diffraction pattern of sample PtG2-16h confirmed the formation of this iron oxide during the α-FeOOH to Fe_3O_4 transformation.

3.3. FT-IR spectroscopy

The FT-IR spectra of the prepared samples in the wave number range from 1100 to 300 cm^{-1} are shown in Figs. 4 and 5. The FT-IR spectra of the samples obtained by up to 6 h of hydrothermal treatment correspond to a single phase α-FeOOH [55–57]. The IR bands at 891 and 796 cm^{-1} correspond to Fe–O–H bending vibrations, whereas the bands at lower wave numbers correspond to Fe–O and Fe–OH stretching vibrations or lattice vibration bands. A longer hydrothermal treatment of the precipitation system (for 16 and 24 h) caused shifts of all these vibration bands due to improved crystallinity and/or changes in the shape of α-FeOOH particles [39]. The appearance of the IR bands at 575 cm^{-1} in the spectrum of sample PtG1-24h (Fig. 4) and at 580 cm^{-1} in the spectrum of samples PtG2-16h and PtG2-24h (Fig. 5) confirmed the presence of Fe_3O_4 in the said samples [58–61]. The above mentioned Fe_3O_4 IR band is dominant in the spectrum of sample PtG1-72h (Fig. 4), which is in line with the dominance of Fe_3O_4 in that sample as observed by Mössbauer spectroscopy and XRD. However, unlike the results of Mössbauer spectroscopy and XRD, the IR spectrum of sample PtG1-72h also contains the characteristic α-FeOOH bands at about 900 and 800 cm^{-1}, which indicates the presence of a small amount of α-FeOOH in that sample. It is a well-known fact that due to the high intensity of these Fe–OH bending bands the IR spectroscopy is a method more sensitive to detect small amounts of α-FeO-OH and other iron oxyhydroxides than XRD or Mössbauer spectroscopy [62–64].

3.4. FE-SEM and EDS

The size and morphology of particles in the samples were observed by FE-SEM and the characteristic images are shown in Figs. 6–8. Reference sample G consists of uniform lath-like α-FeOOH particles 150–200 nm in length (Fig. 6a). The FE-SEM image of sample PtG1-2h formed in the presence of 1 mol% of Pt ions showed the presence of similar lath-like particles (Fig. 6b). The presence of 5 mol% of Pt ions in the precipitation
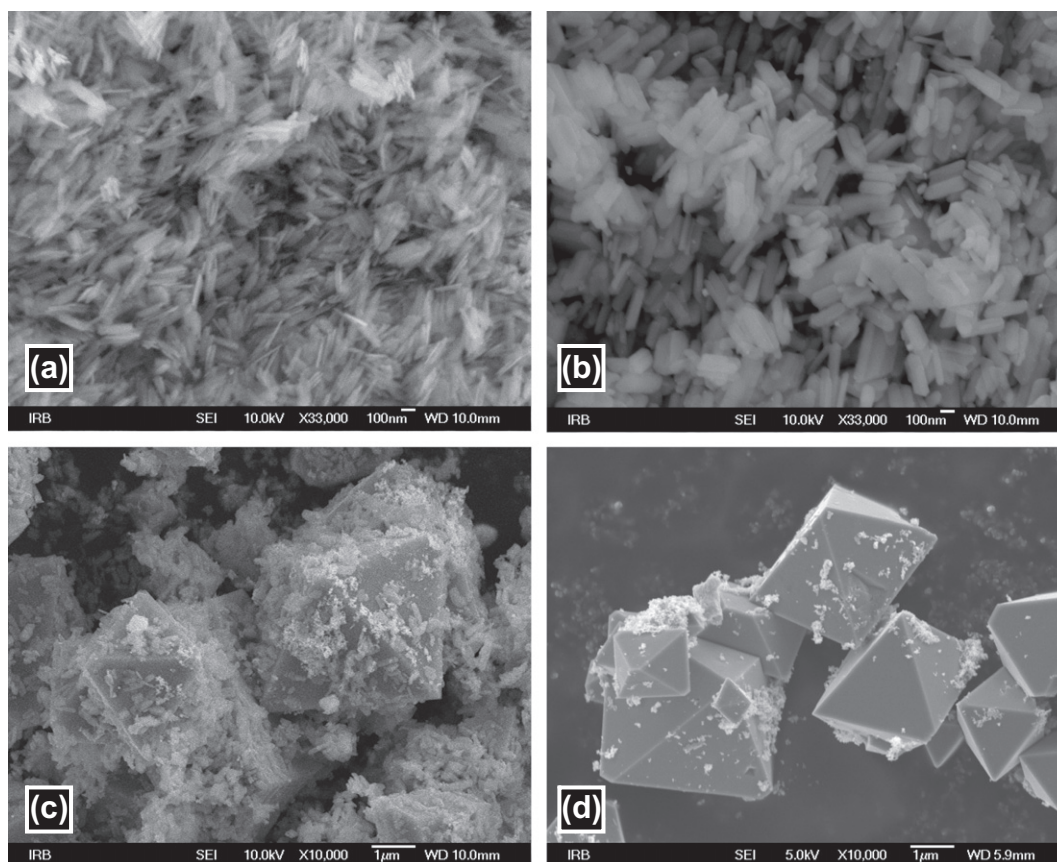
Fig. 7. FE-SEM images of samples: (a) PtG1-6h, (b) PtG1-16h, (c) PtG1-24h and (d) PtG1-72h.
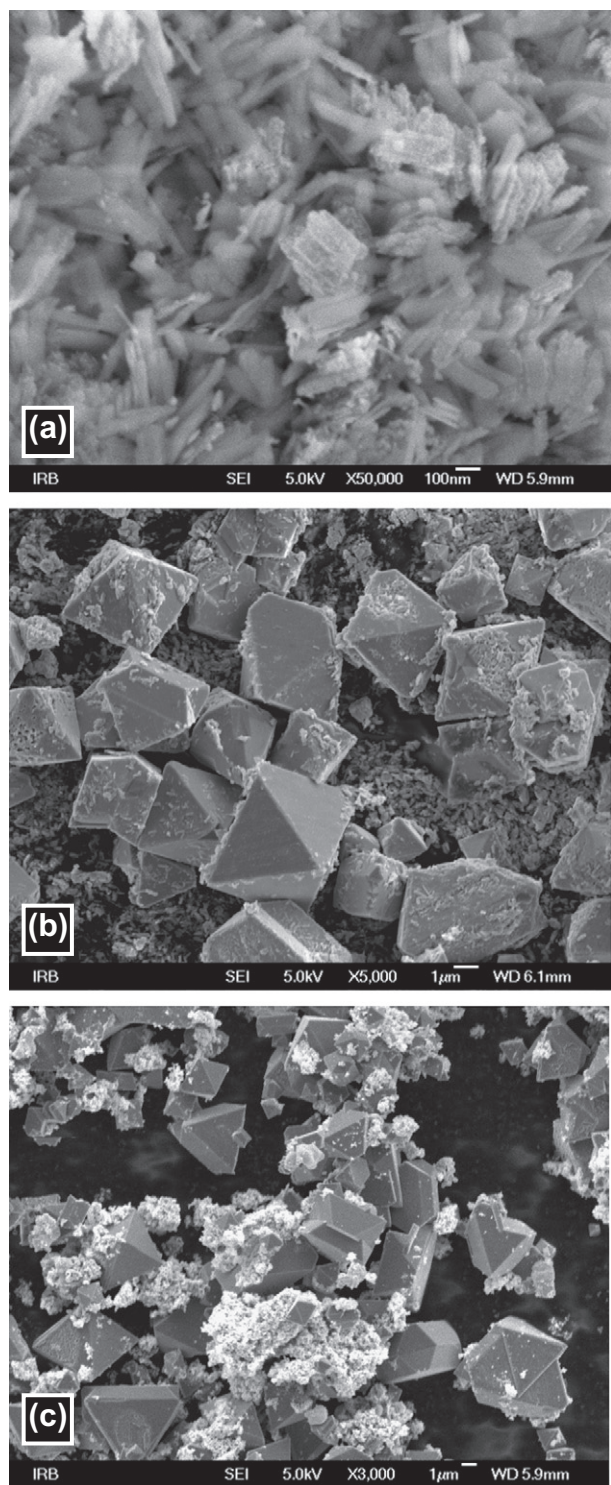
Fig. 8. FE-SEM images of samples: (a) PtG2-6h, (b) PtG2-16h and (c) PtG2-24h.

Fig. 9. EDS analysis of sample PtG2-24h (5 mol% Pt in initial reaction mixture, heating period 24 h): (a) FE-SEM image, (b) EDS analysis of the area in the white rectangle, and (c) EDS analysis of the area in the black rectangle.

system also did not significantly change the size and shape of α-FeOOH lath-like particles (sample PtG1-2h, Fig. 6c) compared to reference sample G.

The FE-SEM image of sample PtG1-6h formed in the presence of 1 mol% of Pt ions (Fig. 7a) showed the presence of lath-like α-FeOOH particles similar to particles in reference sample G (Fig. 6a). A longer hydrothermal treatment of the system (sample PtG1-16h, Fig. 7b) results in larger and thicker α-FeOOH lath-like particles of better crystallinity due to the aggregation and growth of initially

formed α-FeOOH particles. Nanoparticles of metallic platinum are well visible in the FE-SEM image of that sample. The FE-SEM image of sample PtG1-24h (Fig. 7c) showed the presence of Fe$_3$O$_4$ octahedral crystals of a few micrometers in size, lath-like α-FeOOH particles and coalesced α-FeOOH particles of about 150–200 nm in length, and metallic platinum nanoparticles located at the surface of Fe$_3$O$_4$ or α-FeOOH particles. Hydrothermal treatment for 72 h resulted in an almost complete transformation of α-FeOOH particles to Fe$_3$O$_4$ octahedral crystals in the presence of platinum nanoparticles (Fig. 7d).

Unlike the sample PtG1-6h (Fig. 7a), the sample obtained after 6 h of autoclaving in the presence of 5 mol% of Pt showed the presence of platinum nanoparticles formed on the surface of α-FeOOH laths (Fig. 8a). The FE-SEM image of the sample obtained after 16 h (Fig. 8b) showed the presence of micrometer-size Fe$_3$O$_4$ octahedral particles, platinum nanoparticles and a small amount of α-FeOOH laths. These α-FeOOH particles disappeared in the FE-SEM image of sample PtG2-24h (Fig. 8c) due to the transformation to Fe$_3$O$_4$.

Micrometer-size Fe_3O_4 octahedral particles and platinum nanoparticles were visible. The elemental composition of the particles was revealed by EDS (Fig. 9). It was confirmed that the micrometer-size octahedral particles correspond to Fe_3O_4 and the nanoparticles correspond to platinum.

The formation of platinum nanoparticles and the transformation of α-FeOOH to Fe_3O_4 can be presented by formal chemical equations:

$$Pt(OH)_6^{2-} + 4e^- \rightarrow Pt^0 + 6OH^-$$

$$3\alpha\text{-FeOOH} + e^- \xrightarrow{Pt} Fe_3O_4 + H_2O + OH^-$$
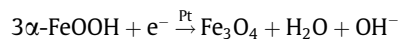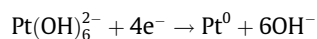
The source of electrons for the above mentioned reduction reactions is TMAH and the products of its thermal decomposition (methanol and trimethylamine). For the reduction of ferric iron in α-FeOOH to ferrous iron in Fe_3O_4 in this system the presence of a platinum group metal catalyst is necessary [45,49,59,65]. Without the presence of the platinum group metal nanoparticles the transformation of α-FeOOH to Fe_3O_4 in the presence of TMAH and its thermal decomposition products has not been obtained, even in very long hydrothermal treatments [39].

4. Conclusions

- A strong influence of the presence of platinum(IV) ions, similar to cations of other platinum group metals, on the formation of iron oxides in a highly alkaline medium in the presence of tetramethylammonium hydroxide was observed.
- In the presence of Pt ions lath-like α-FeOOH particles were formed. In their shape and size these particles were similar to the particles in the reference sample. However, the presence of Pt ions in the precipitation system led to the formation of α-FeOOH crystallites of lower mean size. A possibility of minor incorporation of Pt ions into the α-FeOOH structure was suggested on the basis of Mössbauer spectroscopy and XRD results.
- A longer hydrothermal treatment led to the formation of platinum nanoparticles by reduction of Pt(IV) ions with TMAH and the products of its thermal decomposition.
- These platinum nanoparticles catalyzed the transformation of α-FeOOH to Fe_3O_4 in the presence of TMAH and its thermal decomposition products as a source of electrons necessary for the reduction of ferric iron.

References

[1] R.M. Cornell, U. Schwertmann, The Iron Oxides, Structure, Properties, Reactions, Occurrence and Uses, Wiley-VCH, 2003.
[2] Y. Tardy, D. Nahon, Am. J. Sci. 285 (1985) 865.
[3] U. Schwertmann, L. Carlson, Soil Sci. Soc. Am. J. 58 (1994) 256.
[4] A. Manceau, M.L. Schlegel, M. Musso, V.A. Sole, C. Gauthier, P.E. Petit, F. Trolard, Geochim. Cosmochim. Acta 64 (2000) 3643.
[5] M. Landers, R.J. Gilkes, Appl. Clay Sci. 35 (2007) 162.
[6] J.C.Ø. Andersen, G.K. Rollinson, B. Snook, R. Herrington, R.J. Fairhurst, Miner. Eng. 22 (2009) 1119.
[7] K. Inouye, S. Ishii, K. Kaneko, T. Ishikawa, Z. Anorg. Allg. Chem. 391 (1972) 86.
[8] R.M. Cornell, Clay Miner. 23 (1988) 329.
[9] R. Giovanoli, R.M. Cornell, Z. Pflanzenernähr. Bodenk. 155 (1992) 455.
[10] T. Nagano, H. Mitamura, S. Nakayama, S. Nakashima, Clays Clay Miner. 47 (1999) 748.
[11] Q. Liu, K. Osseo-Asare, J. Colloid Interf. Sci. 231 (2000) 401.
[12] S. Krehula, S. Musić, J. Mol. Struct. 834–836 (2007) 154.
[13] S. Krehula, S. Musić, Mater. Chem. Phys. 123 (2010) 67.
[14] U. Schwertmann, U. Gasser, H. Sticher, Geochim. Cosmochim. Acta 53 (1989) 1293.
[15] J. Gerth, Geochim. Cosmochim. Acta 54 (1990) 363.
[16] F.J. Berry, Ö. Helgason, A. Bohórquez, J.F. Marco, J. McManus, E.A. Moore, S. Mørup, J. Mater. Chem. 10 (2000) 1643.
[17] C.A. dos Santos, A.M.C. Horbe, C.M.O. Barcellos, J.B. Marimon da Cunha, Solid State Commun. 118 (2001) 449.
[18] N. Kaur, B. Singh, B.J. Kennedy, M. Gräfe, Geochim. Cosmochim. Acta 73 (2009) 582.
[19] T. Fujii, M. Kayano, Y. Takada, M. Nakanishi, J. Takada, Solid State Ionics 172 (2004) 289.
[20] W.B. Ingler Jr., S.U.M. Khan, Thin Solid Films 461 (2004) 301.
[21] Y. Kubota, H. Morita, Y. Tokuoka, Y. Imaoka, IEEE Trans. Magn. 15 (1979) 1558.
[22] M.A. Wells, R.W. Fitzpatrick, R.J. Gilkes, J. Dobson, Geophys. J. Int. 138 (1999) 571.
[23] J. Lai, K.V.P.M. Shafi, K. Loos, A. Ulman, Y. Lee, T. Vogt, C. Estournès, J. Am. Chem. Soc. 125 (2003) 11470.
[24] C. Sudakar, G.N. Subbanna, T.R.N. Kutty, J. Mater. Sci. 39 (2004) 4271.
[25] M.A. Wells, R.J. Gilkes, R.W. Fitzpatrick, Clays Clay Miner. 49 (2001) 60.
[26] I.R. Guimaraes, A. Giroto, L.C.A. Oliveira, M.C. Guerreiro, D.Q. Lima, J.D. Fabris, Appl. Catal. B: Environ. 91 (2009) 581.
[27] E. Subramanian, J.-O. Baeg, S.M. Lee, S.-J. Moon, K.-J. Kong, Int. J. Hydrogen Energy 34 (2009) 8485.
[28] W.F. de Souza, I.R. Guimarães, L.C.A. Oliveira, A.S. Giroto, M.C. Guerreiro, C.L.T. Silva, Appl. Catal., A 381 (2010) 36.
[29] S. Mustafa, S. Khan, M.I. Zaman, S.Y. Husain, Appl. Surf. Sci. 255 (2009) 8722.
[30] S. Mustafa, S. Khan, M.I. Zaman, Water Res. 44 (2010) 918.
[31] J.Z. Jiang, R. Lin, W. Lin, K. Nielsen, S. Mørup, K. Dam-Johansen, R. Clasen, J. Phys. D: Appl. Phys. 30 (1997) 1459.
[32] O.K. Tan, W. Cao, Y. Hu, W. Zhu, Ceram. Int. 30 (2004) 1127.
[33] Y. Wang, F. Kong, B. Zhu, S. Wang, S. Wu, W. Huang, Mater. Sci. Eng. B 140 (2007) 98.
[34] C. Sudakar, G.N. Subbanna, T.R.N. Kutty, J. Mater. Chem. 12 (2002) 107.
[35] Y.-S. Hu, A. Kleiman-Shwarscstein, A.J. Forman, D. Hazen, J.-N. Park, E.W. McFarland, Chem. Mater. 20 (2008) 3803.
[36] I.-S. Lim, G.-E. Jang, C.K. Kim, D.-H. Yoon, Sensors Actuat. B 77 (2001) 215.
[37] V.K. Tzitzios, D. Petridis, I. Zafiropoulou, G. Hadjipanayis, D. Niarchos, J. Magn. Magn. Mater. 294 (2005) e95.
[38] S. Krehula, S. Popović, S. Musić, Mater. Lett. 54 (2002) 108.
[39] S. Krehula, S. Musić, J. Cryst. Growth 310 (2008) 513.
[40] D.M.E. Thies-Weesie, Chem. Mater. 19 (2007) 5538.
[41] E. Van den Pol, D.M.E. Thies-Weesie, A.V. Petukhov, G.J. Vroege, K. Kvashnina, J. Chem. Phys. 129 (2008) 164715.
[42] Q. Wang, M. Yang, Y. Chen, Key Eng. Mater. 336–338 (2007) 2218.
[43] S. Krehula, S. Musić, S. Popović, Ž. Skoko, J. Alloys Compd. 420 (2006) 260.
[44] S. Krehula, S. Musić, J. Alloys Compd. 431 (2007) 56.
[45] S. Krehula, S. Musić, J. Mol. Struct. 924–926 (2009) 201.
[46] B. Rupp, Scripta Metall. 22 (1988) 1.
[47] D.G. Schulze, U. Schwertmann, Clay Miner. 19 (1984) 521.
[48] H.P. Klug, L.E. Alexander, X-Ray Diffraction Procedures for Polycrystalline and Amorphous Materials, Wiley, 1974. p. 687.
[49] S. Krehula, S. Musić, J. Mol. Struct. 976 (2010) 61.
[50] E. Murad, J.H. Johnston, Iron Oxides and Oxyhydroxides, in: G.J. Long (Ed.), Mössbauer Spectroscopy Applied to Inorganic Chemistry, vol. 2, Plenum Publishing Corporation, 1987, p. 507.
[51] E. Murad, U. Schwertmann, Clay Miner. 18 (1983) 301.
[52] C.A. Barrero, R.E. Vandenberghe, E. De Grave, Hyperfine Interact. 122 (1999) 39.
[53] M. Gotić, G. Koščec, S. Musić, J. Mol. Struct. 924–926 (2009) 347.
[54] R.D. Shannon, Acta Crystallogr. A32 (1976) 751.
[55] L. Verdonck, S. Hoste, F.F. Roelandt, G.P. van der Kelen, J. Mol. Struct. 79 (1982) 273.
[56] P. Cambier, Clay Miner. 21 (1986) 191.
[57] P. Cambier, Clay Miner. 21 (1986) 201.
[58] M. Ishii, M. Nakahira, T. Yamanaka, Solid State Commun. 11 (1972) 209.
[59] S. Krehula, S. Musić, Croat. Chem. Acta 80 (2007) 517.
[60] M. Gotić, S. Musić, J. Mol. Struct. 834–836 (2007) 445.
[61] M. Gotić, T. Jurkin, S. Musić, Mater. Res. Bull. 44 (2009) 2014.
[62] A. Šarić, S. Musić, K. Nomura, S. Popović, J. Mol. Struct. 480–481 (1999) 633.
[63] M. Ristić, S. Musić, M. Godec, J. Alloys Compd. 417 (2006) 292.
[64] M. Žic, M. Ristić, S. Musić, J. Mol. Struct. 924–926 (2009) 235.
[65] S. Krehula, S. Musić, J. Alloys Compd. 416 (2006) 284.